INTERNATIONAL JOURNAL FOR NUMERICAL METHODS IN ENGINEERING
Int. J. Numer. Meth. Engng 2005; **64**:877–906
Published online 14 June 2005 in Wiley InterScience (www.interscience.wiley.com). DOI: 10.1002/nme.1385

A new boundary element technique without domain integrals for elastoplastic solids

Katia Bertoldi[‡], Michele Brun[§] and Davide Bigoni[*, †]

Dipartimento di Ingegneria Meccanica e Strutturale, Università di Trento, Via Mesiano 77-38050 Povo, Trento, Italia

SUMMARY

A simple idea is proposed to solve boundary value problems for elastoplastic solids via boundary elements, namely, to use the Green's functions corresponding to *both* the loading and unloading branches of the tangent constitutive operator to solve for plastic and elastic regions, respectively. In this way, domain integrals are completely avoided in the boundary integral equations. Though a discretization of the region where plastic flow occurs still remains necessary to account for the inhomogeneity of plastic deformation, the elastoplastic analysis reduces, in essence, to a straightforward adaptation of techniques valid for anisotropic linear elastic constitutive equations (the loading branch of the elastoplastic constitutive operator may be viewed formally as a type of anisotropic elastic law). Numerical examples, using J_2-flow theory with linear hardening, demonstrate that the proposed method retains all the advantages related to boundary element formulations, is stable and performs well.

The method presented is for simplicity developed for the associative flow rule; however, a full derivation of Green's function and boundary integral equations is also given for the general case of non-associative flow rule. It is shown that in the non-associative case, a domain integral unavoidably arises in the formulation. Copyright © 2005 John Wiley & Sons, Ltd.

KEY WORDS: Green's function; boundary integral equations; boundary elements; elastoplasticity; domain integrals

1. INTRODUCTION

Boundary element techniques in elastoplasticity, pioneered by Swedlow and Cruse [1], Mukherjee [2], Maier [3], and Telles [4], present well-known advantages (volume discretization of only

*Correspondence to: D. Bigoni, Dipartimento di Ingegneria Meccanica e Strutturale, Università di Trento, Via Mesiano 77, I-38050 Trento, Italia.
†E-mail: bigoni@ing.unitn.it, URL: http://www.ing.unitn.it/∼bigoni/
‡E-mail: katia.bertoldi@ing.unitn.it
§E-mail: michele.brun@ing.unitn.it

Contract/grant sponsor: MURST-Cofin 2004; contract/grant number: 2004083253_002

Received 22 September 2004
Revised 28 January 2005
Accepted 18 April 2005

the plastic zone, easy treatment of incompressibility, singularities and infinite domains) when compared to other numerical techniques such as finite elements and have been successfully applied to solve boundary value problems in a number of complex situations. Examples include sensitivity analyses [5], dynamical loadings [6, 7], shear band formation [8], gradient plasticity [9, 10], thermo-elasto-plasticity [11], and large strains [12–16].

Thus, the boundary element approach to elastoplasticity should be considered a field which has reached a significant level of maturity. Nevertheless, a central problem remains open. In particular, following the standard approach, volume integrals appear in the governing integral equations, containing hypersingular terms multiplied by the unknown plastic strain rate field (see for instance Reference [17]). These strong singularities complicate the formulation and are difficult to treat, both numerically and analytically [18], so that the exploration of possible remedies to this problem has generated an intense research effort (see the discussion by Gao and Davis [19]).

Two approaches to avoid volume integrations are particularly relevant to the present discussion. In one approach, domain integrals are reduced to surface integrals along the boundaries of the cells in which the plastic domain is divided [19, 20]. In the other approach, special surface integrals take into account the non-linear effects due to plasticity [21]. The two methods certainly represent important steps towards the solution of the problem, but require an *ad hoc* and somewhat complicated analytical and numerical treatments and laborious implementation.

The objective of the present article is to propose a new approach to boundary elements in elastoplasticity, retaining all advantages typical of these formulations, but avoiding domain integrals. Consequently, though a volume discretization remains necessary to account for the inhomogeneity of plastic deformation, the implementation simplifies drastically when compared to the other techniques currently in use. The presented methodology traces back to Brun *et al*. [22, 23] who pointed out that the use of a Green's function defined for incremental deformation leads to a boundary integral formulation for *homogeneous* finite deformation in which domain integrals are simply absent. With reference to small strain theory of associative elastoplasticity, the purpose of the present article is to show:

(i) a generalization of the Brun *et al*. [22, 23] approach to attack problems involving inhomogeneous deformation;
(ii) that the approach is general enough to be applicable to a broad class of constitutive models;
(iii) the main advantages and limitations of the approach;
(iv) that when tested on specific numerical problems the approach yields stable results and performs correctly.

Elaborating on Point (i), the main ideas to solve elastoplastic problems are the following.

(1) Let us refer to an elastoplastic material, defined by a piecewise linear tangent constitutive operator, different in loading and unloading.
(2) Suppose that both the Green's functions for incremental loading and unloading, together with the relevant boundary integral equations, are available for homogeneous response.
(3) It follows that—as explicitly shown by Bigoni and Capuani [24] and Brun *et al*. [22, 23], with reference to non-linear elasticity—incremental boundary value problems superimposed on a homogeneous state can be solved via boundary elements, without domain integrals. Through integration along a loading path, finite homogeneous deformations can

be analysed. Note that different integration schemes can be adopted (a simple forward-Euler integration approach was employed in Reference [22], but more complicated iterative procedures can obviously be introduced. In the present case of elastoplasticity we will propose a Newton–Raphson iterative method based on a cutting-plane return mapping algorithm).

(4) Let us consider a generic (involving inhomogeneous deformations) boundary value problem, where a solid is assumed to be divisible into sufficiently small volume elements to be treated using a Green's function relative to a homogeneous material. Note that the volume discretization can be considered *a priori* defined, but can also be allowed to vary from step to step as a function of the current detected inhomogeneities.

(5) The incremental response of the elements defined in (4) is characterized by either an unloading or loading operator and can be solved for each element making recourse to the boundary element technique mentioned in (3). Through consideration of all elements, namely, employing a multizone technique, and integration along a prescribed loading path, a generic boundary value problem can be numerically solved.

Regarding Point (ii), following References [25, 26], we provide a general formula for the quasi-static, infinite-body Green's function for two-dimensional incremental deformation of a generic material,[¶] including the tangent operator of elastoplasticity and damage *with a non-associative flow rule* (Section 2). The Green's function is given in an arbitrary reference system, so that there is no need for rotating references during solution of boundary value problems. We also derive the relevant boundary integral equations for velocity, deformation and stress rates. This derivation provides evidence of a peculiarity of the proposed method: as related to the non-associativity of the flow rule, the boundary integral equation for velocity contains a volume term related to the lack of major symmetry of the tangent constitutive operator. Therefore, to completely avoid domain integrals, we restrict the analysis to the associative case. This observation anticipates issues concerned with Point (iii), so that we conclude our method, at the level of generality presented here, to be restricted to associative plasticity and the elliptic regime.

Difficulties in the implementation of our method are related to numerical integrations of the Green's function and to the fact that a large and sparse coefficient matrix is obtained for the final solving system. The problem connected to the sparsity has been successfully circumvented by employing the technique developed by Zlatev *et al*. [29], to treat sparse systems of linear algebraic equations by Gaussian elimination. Numerical integrations were performed by simply employing a standard Gauss integration, so that computing times were observed to blow up at the increase of the discretization. Obviously, further development of the proposed method requires an optimization of integration[‖] and a parallelization of the code.

[¶]Note that more complex formulations involving dynamical loading and inhomogeneous deformation can also be developed following Reference [26]. For instance, the Green's functions for the loading branch of certain elastoplastic material classes have been derived in References [27, 28], under the assumption of time-harmonic vibrations.

[‖]Results obtained when the present article was already submitted, and restricted to the constitutive context analysed in References [22, 24], have revealed a new direct way for obtaining the Green's tractions with a drastic simplification of the related numerical integrations [30]. These new results, still to be tested, could remarkably improve the numerical performance of the method proposed in the present article.

The main advantage of the proposed method is that it does not require development of special calculations and related routines, but it reduces in essence to a systematic use of linear solutions or, in other words, to techniques akin to those employed for linear, inhomogeneous anisotropic elasticity.

Finally, regarding Point (iv), to test the validity of our approach, we present a series of examples referred to the challenging problem of incompressible elastic and plastic deformations. It is shown that problems related to critical situations such those investigated by Nagtegaal *et al*. [31] and Cervera *et al*. [32] are 'naturally' avoided and results are quite satisfactory, so that our technique is proven to be robust and accurate.

2. GREEN'S FUNCTION FOR TWO-DIMENSIONAL, QUASI-STATIC PROBLEMS

Since the development of the methodology proposed in this article requires the determination of the infinite-body Green's function for the loading and unloading branches of the constitutive equation, this section is devoted to the presentation of a general technique to obtain this for *quasi-static*, *two-dimensional problems in the elliptic regime*. The approach to Green's functions that will be followed was originally proposed for elastic solids by Willis [25, 26] and is detailed below with reference to different laws of elasticity and plasticity.

Let us start by considering the equilibrium equations of a generic body characterized by a linear operator $\mathbb{C}$ relating stress to the displacement gradient $\nabla\mathbf{u}$

$$\operatorname{div}(\mathbb{C}[\nabla\mathbf{u}]) + \mathbf{f} = \mathbf{0} \tag{1}$$

where $\mathbf{f}$ denotes the body force. The fundamental solution or Green's function is the general solution of Equation (1) to a concentrated force $\mathbf{f}^g = \mathbf{e}^g\delta(\mathbf{x})$ acting at the origin $\mathbf{x} = \mathbf{0}$ in the direction singled out by the unit vector $\mathbf{e}^g$, where $\delta(\mathbf{x})$ is the two-dimensional Dirac delta function. Note that upon introducing an orthogonal reference system, the unit vector becomes the Kronecker delta $e_i^g = \delta_{ig}$.

The solution to the above problem is obtained by employing a plane wave expansion [33], which for a generic function h is written as

$$h(\mathbf{x}) = -\frac{1}{4\pi^2}\oint_{|\mathbf{n}|=1}\tilde{h}(\mathbf{n}\bullet\mathbf{x})\,\mathrm{d}\mathbf{n} \tag{2}$$

where $\mathbf{n}$ is the radial unit vector centred at the origin of the position vector $\mathbf{x}$.

Since in the transformed domain the following properties hold:

$$\tilde{\delta}(\mathbf{n}\bullet\mathbf{x}) = \frac{1}{(\mathbf{n}\bullet\mathbf{x})^2}, \quad \nabla_{\mathbf{x}}\tilde{h}(\mathbf{n}\bullet\mathbf{x}) = \tilde{h}'(\mathbf{n}\bullet\mathbf{x})\mathbf{n} \tag{3}$$

where the prime denotes differentiation with respect to the argument $\mathbf{n}\bullet\mathbf{x}$, the equilibrium equation (1) becomes

$$\mathbf{A}(\mathbf{n})(\tilde{\mathbf{u}}^g)'' + \mathbf{e}^g\tilde{\delta} = \mathbf{0} \tag{4}$$

where the acoustic tensor $\mathbf{A}(\mathbf{n})$ is defined for every vector $\mathbf{g}$ as

$$\mathbf{A}(\mathbf{n})\mathbf{g} = \mathbb{C}[\mathbf{g}\otimes\mathbf{n}]\mathbf{n} \tag{5}$$

Equation (4) can now be integrated if the acoustic tensor is not singular, $\det \mathbf{A}(\mathbf{n}) \neq 0$ for all unit vectors $\mathbf{n}$—or, in equivalent words, *when the problem is elliptic*—yielding

$$\tilde{\mathbf{u}}^g(\mathbf{n}\bullet\mathbf{x}) = \mathbf{A}^{-1}(\mathbf{n})\mathbf{e}^g \log|\mathbf{n}\bullet\hat{\mathbf{x}}| \tag{6}$$

where linear and constant terms in $\mathbf{n}\bullet\mathbf{x}$ have been neglected and $\hat{\mathbf{x}}$ is a dimensionless measure of $\mathbf{x}$.

The Green's function can now be obtained by inverse-transforming Equation (6) to obtain

$$\mathbf{u}^g(\mathbf{x}) = -\frac{1}{4\pi^2}\oint_{|\mathbf{n}|=1} \mathbf{A}^{-1}(\mathbf{n})\mathbf{e}^g \log|\mathbf{n}\bullet\hat{\mathbf{x}}|\,\mathrm{d}\mathbf{n} \tag{7}$$

Introducing the radial (dimensionless) measure of the distance $\hat{r} = |\hat{\mathbf{x}}|$, the angle α between vectors $\mathbf{n}$ and $\mathbf{x}$ and the angle θ singling out $\mathbf{x}$ with respect to x_1-axis, the Green's function (7) can be expressed as

$$\mathbf{u}^g(\hat{r},\theta) = -\frac{\log\hat{r}}{4\pi^2}\int_0^{2\pi} \mathbf{A}^{-1}(\mathbf{n})\mathbf{e}^g\,\mathrm{d}\alpha - \frac{1}{4\pi^2}\int_0^{2\pi} \mathbf{A}^{-1}(\mathbf{n})\mathbf{e}^g\,\log|\cos\alpha|\,\mathrm{d}\alpha \tag{8}$$

where it can be noted that the singularity is explicit and the spectral representation of the acoustic tensor is not needed.

Remark 1

The Green's function (8) is symmetric if and only if $\mathbf{A}(\mathbf{n})$, which in plasticity occurs for associative flow rule is

$$u_i^g = u_g^i \iff A_{ij}(\mathbf{n}) = A_{ji}(\mathbf{n}) \iff \mathbb{C}_{ijhk} = \mathbb{C}_{hkij} \Longleftarrow \text{associativity}$$

$$u_i^g \neq u_g^i \iff A_{ij}(\mathbf{n}) \neq A_{ji}(\mathbf{n}) \iff \mathbb{C}_{ijhk} \neq \mathbb{C}_{hkij} \Longleftarrow \text{non-associativity}$$

The Green's displacement gradient $\nabla\mathbf{u}^g$ can be obtained for internal points either directly by differentiation of the Green's displacement $\mathbf{u}^g$ or by differentiation and subsequent transformation of $\tilde{\mathbf{u}}^g$, yielding in both cases

$$\nabla\mathbf{u}^g = -\frac{1}{4\pi^2}\oint_{|\mathbf{n}|=1} \mathbf{A}^{-1}(\mathbf{n})\mathbf{e}^g \otimes \frac{\mathbf{n}}{\mathbf{n}\bullet\mathbf{x}}\,\mathrm{d}\mathbf{n} \tag{9}$$

Finally, application of the constitutive tensor $\mathbb{C}$ to $\nabla\mathbf{u}^g$ gives the Green's Cauchy stress

$$\boldsymbol{\sigma}^g = -\frac{1}{4\pi^2}\oint_{|\mathbf{n}|=1} \mathbb{C}\left[\mathbf{A}^{-1}(\mathbf{n})\mathbf{e}^g \otimes \frac{\mathbf{n}}{\mathbf{n}\bullet\mathbf{x}}\right]\mathrm{d}\mathbf{n} \tag{10}$$

It is important to note that the Green's function (7) or (8) and all related quantities (9) and (10) are defined for a generic acoustic tensor $\mathbf{A}(\mathbf{n})$, and thus also unsymmetric, as in the case for elastoplasticity with non-associative flow rule, a situation that will be discussed in detail later.

Remark 2
When the border of loss of ellipticity is approached, one eigenvalue of $\mathbf{A}(\mathbf{n})$ goes to zero, so that the integrals in Equations (8)–(10) tend to become singular. This important circumstance is *linked to the appearance of shear bands* and it has been thoroughly investigated by Bigoni and Capuani [24, Appendix A].

As an explanation of how to employ the above technique for obtaining Green's functions, the simple example of linear isotropic elasticity is given in Appendix A.

2.1. The incompressible case

The treatment of materials with internal constraints requires an *ad hoc* formulation; limiting attention here to the incompressibility constraint, problem (1) is reformulated as

$$\operatorname{div}(\mathbb{C}[\nabla\mathbf{u}]) + \nabla p + \mathbf{f} = \mathbf{0}, \quad \operatorname{div}\mathbf{u} = 0 \tag{11}$$

where $p = \operatorname{tr}(\boldsymbol{\sigma})/3$ is the pressure.

As for the case of compressibility, transformation (2) is applied, so that by introducing the representations

$$\tilde{\mathbf{u}}^g = -\gamma^g \mathbf{l} \log|\mathbf{n}\cdot\hat{\mathbf{x}}|, \quad \tilde{p}^g = -q^g \frac{\partial(\log|\mathbf{n}\cdot\hat{\mathbf{x}}|)}{\partial(\mathbf{n}\cdot\mathbf{x})} = -q^g \frac{1}{\mathbf{n}\cdot\mathbf{x}} \tag{12}$$

into Equations (11), where γ^g and q^g are two scalars and $\mathbf{l}$ is a unit vector, we obtain

$$\gamma^g \mathbf{A}\mathbf{l} + q^g \mathbf{n} + \mathbf{e}^g = \mathbf{0}, \quad \mathbf{l}\cdot\mathbf{n} = 0 \tag{13}$$

where $\mathbf{A}$ is the acoustic tensor defined by Equation (5) and is assumed now for simplicity to be symmetric.** In addition, we assume ellipticity, so that for every mutually orthogonal pair of unit vectors $\mathbf{n}$ and $\mathbf{l}$ (such that $\mathbf{n}\cdot\mathbf{l} = 0$)

$$\mathbf{A}(\mathbf{n})\mathbf{l} \neq \mathbf{0}, \iff \mathbf{l}\cdot\mathbf{A}(\mathbf{n})\mathbf{l} \neq 0 \tag{14}$$

Scalar multiplication of Equation $(13)_1$ by $\mathbf{l}$ yields γ^g and subsequent substitution into Equation $(13)_1$ provides q^g

$$\gamma^g = -\frac{\mathbf{e}^g\cdot\mathbf{l}}{\mathbf{l}\cdot\mathbf{A}\mathbf{l}}, \quad q^g = -\mathbf{e}^g\cdot\mathbf{n} + \frac{\mathbf{e}^g\cdot\mathbf{l}}{\mathbf{l}\cdot\mathbf{A}\mathbf{l}}\mathbf{n}\cdot\mathbf{A}\mathbf{l} \tag{15}$$

Having determined γ^g and q^g, the Green's function set $\{\mathbf{u}^g, p^g\}$ can be obtained by anti-transforming Equation (12), namely,

$$\begin{cases} \mathbf{u}^g(\mathbf{x}) = -\dfrac{1}{4\pi^2}\displaystyle\oint_{|\mathbf{n}|=1} \frac{\mathbf{e}^g\cdot\mathbf{l}}{\mathbf{l}\cdot\mathbf{A}\mathbf{l}}\mathbf{l}\log|\mathbf{n}\cdot\hat{\mathbf{x}}|\,\mathrm{d}\mathbf{n} \\ p^g(\mathbf{x}) = -\dfrac{1}{4\pi^2}\displaystyle\oint_{|\mathbf{n}|=1} \left(\mathbf{e}^g\cdot\mathbf{n} - \frac{\mathbf{e}^g\cdot\mathbf{l}}{\mathbf{l}\cdot\mathbf{A}\mathbf{l}}\mathbf{n}\cdot\mathbf{A}\mathbf{l}\right)\frac{1}{\mathbf{n}\cdot\mathbf{x}}\,\mathrm{d}\mathbf{n} \end{cases} \tag{16}$$

**Models of elastoplasticity equipped with incompressibility and non-associative flow rule are extremely rare. An example can be found in Reference [34].

where, in the two-dimensional case,

$$\mathbf{n} = \{\cos\theta, \sin\theta\}, \quad \mathbf{l} = \{-\sin\theta, \cos\theta\} \tag{17}$$

in which θ is the angle between $\mathbf{n}$ and the x_1-axis.

2.2. The Green's function for the loading branch of the elastic–plastic tangent operator with associative and non-associative flow rule

In the framework of small deformations, a generic inviscid elastoplastic constitutive equation relating the rates of stress $\dot{\boldsymbol{\sigma}}$ and strain $\dot{\boldsymbol{\varepsilon}}$ can be written as (see Reference [35] for a general derivation)

$$\dot{\boldsymbol{\sigma}} = \begin{cases} \mathbb{E}[\dot{\boldsymbol{\varepsilon}}] - \dfrac{1}{H}\langle \mathbf{Q} \bullet \mathbb{E}[\dot{\boldsymbol{\varepsilon}}] \rangle \mathbb{E}[\mathbf{P}] & \text{if } f(\boldsymbol{\sigma}, \mathscr{K}) = 0 \\ \mathbb{E}[\dot{\boldsymbol{\varepsilon}}] & \text{if } f(\boldsymbol{\sigma}, \mathscr{K}) < 0 \end{cases} \tag{18}$$

where $\mathbb{E}$ is the elastic constitutive fourth-order tensor, $\mathscr{K}$ denotes a generic set of internal variables, f is the yield function, $\mathbf{Q}$ and $\mathbf{P}$ are the yield function and plastic potential gradients, so that the case of the associative flow rule corresponds to $\mathbf{P} = \mathbf{Q}$. The Macaulay brackets operator $\langle\cdot\rangle$ is defined for every scalar α so that $\langle\alpha\rangle = (\alpha + |\alpha|)/2$ and represents the source of the incremental non-linearity typical of plasticity. The scalar $H > 0$ is the plastic modulus, related to the hardening modulus h through

$$H = h + \mathbf{Q} \bullet \mathbb{E}[\mathbf{P}] \tag{19}$$

The acoustic tensor corresponding to the loading branch of the constitutive equation (18) can be cast in the form

$$\mathbf{A}_{\mathrm{ep}}(\mathbf{n}) = \mathbf{A}_{\mathrm{e}}(\mathbf{n}) - \frac{1}{H}\mathbf{p}(\mathbf{n}) \otimes \mathbf{q}(\mathbf{n}) \tag{20}$$

where $\mathbf{A}_{\mathrm{e}}$ defined as in (5) with $\mathbb{C}$ replaced by $\mathbb{E}$ is the elastic acoustic tensor, and $\mathbf{p}$ and $\mathbf{q}$ are the two following vectorial functions of $\mathbf{n}$:

$$\mathbf{p}(\mathbf{n}) = \mathbb{E}[\mathbf{P}]\mathbf{n}, \quad \mathbf{q}(\mathbf{n}) = \mathbb{E}[\mathbf{Q}]\mathbf{n} \tag{21}$$

Note that the acoustic tensor (20) is symmetric only in the case of the associative flow rule. Assuming ellipticity of both the elastic, $\det \mathbf{A}_{\mathrm{e}}(\mathbf{n}) \neq 0$, and elastoplastic branch of (18), $H \neq \mathbf{p} \bullet \mathbf{A}_{\mathrm{e}}^{-1}\mathbf{q}$, we have (see e.g. Reference [36])

$$\mathbf{A}_{\mathrm{ep}}^{-1} = \mathbf{A}_{\mathrm{e}}^{-1} + \frac{\mathbf{A}_{\mathrm{e}}^{-1}\mathbf{p} \otimes \mathbf{A}_{\mathrm{e}}^{-1}\mathbf{q}}{H - \mathbf{p} \bullet \mathbf{A}_{\mathrm{e}}^{-1}\mathbf{q}} \tag{22}$$

Obviously, Equation (7) can be reinterpreted in terms of rates, so that a substitution of Equation (22) into Equation (8) yields the plastic branch

$$\mathbf{v}_{\mathrm{ep}}^{g} = -\frac{1}{4\pi^2} \oint_{|\mathbf{n}|=1} (\mathbf{A}_{\mathrm{e}}^{-1}(\mathbf{n}) + \mathbf{B}_{\mathrm{p}}(\mathbf{n}))\mathbf{e}^{g} \log|\mathbf{n} \bullet \hat{\mathbf{x}}| \, \mathrm{d}\mathbf{n} \tag{23}$$

where

$$\mathbf{B}_{\mathrm{p}} = \frac{\mathbf{A}_{\mathrm{e}}^{-1}(\mathbf{n})\mathbf{p}(\mathbf{n}) \otimes \mathbf{A}_{\mathrm{e}}^{-1}(\mathbf{n})\mathbf{q}(\mathbf{n})}{H - \mathbf{p}(\mathbf{n}) \bullet \mathbf{A}_{\mathrm{e}}^{-1}(\mathbf{n})\mathbf{q}(\mathbf{n})} \tag{24}$$

Remark 3
It is important to note that the Green's function (23) can be written as

$$\mathbf{v}_{\mathrm{ep}}^{g} = \mathbf{v}_{\mathrm{e}}^{g} + \mathbf{v}_{\mathrm{p}}^{g} \tag{25}$$

where $\mathbf{v}_{\mathrm{e}}$ is the Green's function relative to the elastic response and

$$\mathbf{v}_{\mathrm{p}}^{g}(\hat{r}, \theta) = -\frac{\log \hat{r}}{4\pi^2} \int_0^{2\pi} \mathbf{B}_{\mathrm{p}}(\mathbf{n})\mathbf{e}^{g} \, \mathrm{d}\alpha - \frac{1}{4\pi^2} \int_0^{2\pi} \mathbf{B}_{\mathrm{p}}(\mathbf{n})\mathbf{e}^{g} \, \log|\cos\alpha| \, \mathrm{d}\alpha \tag{26}$$

(in which $\mathbf{n}$ is inclined at $\alpha + \theta$ with respect to x_1-axis) can be interpreted as a sort of 'plastic correction'.

We finally remark that the Green's function (25) is defined for both associative $\mathbf{P} = \mathbf{Q}$ and non-associative $\mathbf{P} \neq \mathbf{Q}$ flow rules.

2.3. Green's function for incompressible J_2-flow theory of plasticity

The numerical examples developed to show the capabilities of the proposed method will be referred to the extreme case of a constitutive equation which is both plastically and elastically incompressible. This is a version of the J_2-flow theory of plasticity in the particular cases of linear hardening and incompressible elasticity. The rate constitutive equations must be complemented now by the incompressibility constraint $\operatorname{div} \mathbf{v} = 0$, and become

$$\dot{\boldsymbol{\sigma}} - \dot{p}\mathbf{I} = \begin{cases} 2\mu\dot{\boldsymbol{\varepsilon}} - \dfrac{4\mu^2}{h+\mu}\langle \mathbf{Q} \bullet \dot{\boldsymbol{\varepsilon}} \rangle \mathbf{Q} & \text{if } \sqrt{J_2} - \dfrac{\sigma_0}{\sqrt{3}} = 0 \\ 2\mu\dot{\boldsymbol{\varepsilon}} & \text{if } \sqrt{J_2} - \dfrac{\sigma_0}{\sqrt{3}} < 0 \end{cases} \tag{27}$$

where $\dot{p}$ is the rate of pressure, μ the elastic shear modulus, σ_0 the current value of yielding in uniaxial stress and the yield function gradient and the second invariant of deviatoric stress $\mathbf{S}$ are

$$\mathbf{Q} = \frac{\mathbf{S}}{2\sqrt{J_2}}, \quad J_2 = \frac{1}{2}\mathbf{S} \bullet \mathbf{S} \tag{28}$$

For plane deformations, Equation (27) can be rewritten as

$$\dot{\boldsymbol{\sigma}} - \dot{p}\mathbf{I} = \mathbb{K}\nabla\mathbf{v}^{\mathrm{T}}, \quad \operatorname{div} \mathbf{v} = 0 \tag{29}$$

where

$$\dot{p} = \frac{\dot{\sigma}_{11} + \dot{\sigma}_{22}}{2}, \quad \mathbb{K} = \mu_* \mathbf{M} \otimes \mathbf{M} + \mu \mathbf{N} \otimes \mathbf{N} \tag{30}$$

in which tensors

$$\mathbf{M} = \mathbf{e}_1 \otimes \mathbf{e}_1 - \mathbf{e}_2 \otimes \mathbf{e}_2, \quad \mathbf{N} = \mathbf{e}_1 \otimes \mathbf{e}_2 + \mathbf{e}_2 \otimes \mathbf{e}_1 \tag{31}$$

are defined in the (in-plane) principal reference system of $\mathbf{S}$ through its unit eigenvectors $\mathbf{e}_1$ and $\mathbf{e}_2$ and

$$\mu_* = \frac{\mu h}{\mu + h} \tag{32}$$

which is constant for linear hardening.

The derivation of the Green's function set for the constitutive equation (29) can be obtained either as a particular case of Reference [24], or by employing the technique shown in Section 2.1. Following the latter alternative, we introduce the acoustic tensor in the form

$$\mathbf{A} = \mu_* \bar{\mathbf{n}} \otimes \bar{\mathbf{n}} + \mu \bar{\mathbf{l}} \otimes \bar{\mathbf{l}} \tag{33}$$

where

$$\bar{\mathbf{n}} = (\mathbf{I} - 2\mathbf{e}_2 \otimes \mathbf{e}_2)\mathbf{n} \quad \text{and} \quad \bar{\mathbf{l}} = (\mathbf{I} - 2\mathbf{e}_2 \otimes \mathbf{e}_2)\mathbf{l} \tag{34}$$

so that Equations $(15)_1$ and $(15)_2$ specialize

$$\gamma^g = \frac{\sin(\theta + (1-g)\pi/2)}{\mu - 4(\mu - \mu_*)\sin^2\theta\cos^2\theta} \tag{35}$$

and

$$q^g = -\sin^2\theta(\mu - \mu_*)\sin\theta\cos\theta(\cos^2\theta - \sin^2\theta) \tag{36}$$

respectively. Consequently, the Green's function set $\{v_i^g; \dot{p}^g\}$ can be written in the form given in Reference [22]

$$v_t^g = \frac{1}{2\pi^2}\left\{\frac{\pi\delta_{tg}\log\hat{r}}{[(2-t)\gamma_2 + 1 - t]\sqrt{-\gamma_1} + [(2-t)\gamma_1 + 1 - t]\sqrt{-\gamma_2}} - \int_0^{\frac{\pi}{2}} [K_t^g(\alpha+\theta) + (3-2t)(3-2g)K_t^g(\alpha-\theta)]\log(\cos\alpha)\,\mathrm{d}\alpha\right\} \tag{37}$$

$$\dot{p}^g = -\frac{1}{2\pi r}\left\{\cos\left[\theta - (g-1)\frac{\pi}{2}\right] + \frac{1}{\pi}\int_0^{\pi}\frac{\tilde{K}_g(\alpha+\theta)}{\cos\alpha}\,\mathrm{d}\alpha\right\}$$

where r and θ are the polar co-ordinates singling out the generic point with respect to the origin (where the singularity is centred) and

$$
\begin{aligned}
K_t^g(\alpha) &= \frac{\sin[\alpha + (t-1)\pi/2]\sin[\alpha + (g-1)\pi/2]}{\Lambda(\alpha)} \\
\Lambda(\alpha) &= \mu - 4(\mu - \mu_*)\sin^2\alpha\cos^2\alpha \\
\gamma_{1,2} &= 1 - 2\frac{\mu_*}{\mu} \pm 2\sqrt{\frac{\mu_*}{\mu}\left(\frac{\mu_*}{\mu} - 1\right)} \\
\tilde{K}_g(\alpha) &= K_g^g(\alpha)\cos\left[\alpha + (g-1)\frac{\pi}{2}\right]\Gamma(\alpha) \\
\Gamma(\alpha) &= 2\left(\frac{\mu_*}{\mu} - 1\right)(2\cos^2\alpha - 1)
\end{aligned}
\tag{38}
$$

Note that the usual symbol to denote the Cauchy principal value integral has been introduced in expression $(37)_2$ for $\dot{p}^g$.

3. INTEGRAL EQUATIONS FOR THE LOADING BRANCH OF THE ELASTIC–PLASTIC TANGENT OPERATOR FOR ASSOCIATIVE AND NON-ASSOCIATIVE FLOW RULE

In addition to the infinite-body Green's function, boundary integral equations are needed to develop the boundary element technique. We will refer for generality to the loading branch of the constitutive operator (18) describing non-associative plasticity and reducing to the associative case when $\mathbf{P} = \mathbf{Q}$.

Referring to a finite region $\mathscr{B}$ of closed boundary $\partial\mathscr{B}$, we consider mixed boundary value problems in which velocities $\mathbf{v}$ and traction rates $\dot{\mathbf{t}}$ are prescribed functions defined on separate portions $\partial\mathscr{B}_v$ and $\partial\mathscr{B}_t$ of the boundary $\partial\mathscr{B} = \partial\mathscr{B}_v \cup \partial\mathscr{B}_t$

$$
\mathbf{v} = \bar{\mathbf{v}} \quad \text{on } \partial\mathscr{B}_v, \qquad \dot{\boldsymbol{\sigma}}\mathbf{n} = \bar{\dot{\mathbf{t}}} \quad \text{on } \partial\mathscr{B}_t \tag{39}
$$

The rate equilibrium equations for $\dot{\boldsymbol{\sigma}}$ and $\dot{\boldsymbol{\sigma}}^g$, the latter defined with respect to the source point $\mathbf{y}$ and field point $\mathbf{x}$, are

$$
\operatorname{div}\dot{\boldsymbol{\sigma}}(\mathbf{x}) = \mathbf{0}, \qquad \operatorname{div}\dot{\boldsymbol{\sigma}}^g(\mathbf{x},\mathbf{y}) + \mathbf{e}^g\delta(\mathbf{x}-\mathbf{y}) = \mathbf{0} \tag{40}
$$

so that the following identity holds on the body $\mathscr{B}$ except for a disk $\mathscr{C}_\varepsilon$ (of radius ε) surrounding the singularity point $\mathbf{y}$:

$$
\int_{\mathscr{B}-\mathscr{C}_\varepsilon} [\operatorname{div}\dot{\boldsymbol{\sigma}}(\mathbf{x})\bullet\mathbf{v}^g(\mathbf{x},\mathbf{y}) - \operatorname{div}\dot{\boldsymbol{\sigma}}^g(\mathbf{x},\mathbf{y})\bullet\mathbf{v}(\mathbf{x})]\,\mathrm{d}\mathbf{x} = 0 \tag{41}
$$

Since for every smooth vectorial and tensorial field, respectively $\mathbf{a}$ and $\mathbf{A}$, we have

$$
\mathbf{a}\bullet\operatorname{div}\mathbf{A} = \operatorname{div}(\mathbf{A}^{\mathrm{T}}\mathbf{a}) - \mathbf{A}\bullet\nabla\mathbf{a} \tag{42}
$$

and taking the limit for $\varepsilon \longrightarrow 0$, Equation (41) can be cast in the form

$$
\mathbf{c}^g\bullet\mathbf{v}(\mathbf{y}) = \int_{\partial\mathscr{B}} (\dot{\mathbf{t}}\bullet\mathbf{v}^g - \dot{\mathbf{t}}^g\bullet\mathbf{v})\,\mathrm{d}l_x - \int_{\mathscr{B}} (\dot{\boldsymbol{\sigma}}\bullet\nabla\mathbf{v}^g - \dot{\boldsymbol{\sigma}}^g\bullet\nabla\mathbf{v})\,\mathrm{d}\mathbf{x} \tag{43}
$$

where $\dot{\mathbf{t}} = \dot{\boldsymbol{\sigma}}\mathbf{n}$ is the traction rate at the boundary,

$$\mathbf{c}^g(\mathbf{y}) = \lim_{\varepsilon \to 0} \int_{\partial \mathscr{C}_\varepsilon} \boldsymbol{\sigma}^g(\mathbf{x}, \mathbf{y})\mathbf{n} \, \mathrm{d}l_x \tag{44}$$

is the free-term [22, 24], and $\partial \mathscr{C}_\varepsilon$ is the part of the circle (having radius ε and centred at $\mathbf{y}$) intersecting the region occupied by the continuum. It should be noted that to arrive at Equation (43) we have used the following result:

$$\lim_{\varepsilon \to 0} \int_{\mathscr{B} - \mathscr{C}_\varepsilon} (\dot{\boldsymbol{\sigma}} \bullet \nabla \mathbf{v}^g - \dot{\boldsymbol{\sigma}}^g \bullet \nabla \mathbf{v}) \, \mathrm{d}\mathbf{x} = \int_{\mathscr{B}} (\dot{\boldsymbol{\sigma}} \bullet \nabla \mathbf{v}^g - \dot{\boldsymbol{\sigma}}^g \bullet \nabla \mathbf{v}) \, \mathrm{d}\mathbf{x} \tag{45}$$

which holds true since the Green's stress and velocity gradient have a $1/r$ singularity.

To evaluate the domain integral on the right-hand side of Equation (43), we rewrite the loading branch of Equation (18) in the form

$$\dot{\boldsymbol{\sigma}} = \mathbb{E}[\dot{\boldsymbol{\varepsilon}}] - \mathbb{B}[\dot{\boldsymbol{\varepsilon}}], \quad \mathbb{B} = \frac{1}{H} \mathbb{E}[\mathbf{P}] \otimes \mathbb{E}[\mathbf{Q}] \tag{46}$$

so that

$$\int_{\mathscr{B}} (\dot{\boldsymbol{\sigma}} \bullet \nabla \mathbf{v}^g - \dot{\boldsymbol{\sigma}}^g \bullet \nabla \mathbf{v}) \, \mathrm{d}\mathbf{x} = - \int_{\mathscr{B}} (\dot{\boldsymbol{\varepsilon}}^g \bullet \mathbb{B}[\dot{\boldsymbol{\varepsilon}}] - \dot{\boldsymbol{\varepsilon}} \bullet \mathbb{B}[\dot{\boldsymbol{\varepsilon}}^g]) \, \mathrm{d}\mathbf{x} \tag{47}$$

since $\mathbb{E}$ possesses the major symmetry, whereas $\mathbb{B}$ does not in the non-associative case $\mathbf{P} \neq \mathbf{Q}$.

As a conclusion, we obtain *the boundary integral equation for the velocity*

$$\mathbf{c}^g \bullet \mathbf{v}(\mathbf{y}) = \int_{\partial \mathscr{B}} (\dot{\mathbf{t}} \bullet \mathbf{v}^g - \dot{\mathbf{t}}^g \bullet \mathbf{v}) \, \mathrm{d}l_x + \int_{\mathscr{B}} (\dot{\boldsymbol{\varepsilon}}^g \bullet \mathbb{B}[\dot{\boldsymbol{\varepsilon}}] - \dot{\boldsymbol{\varepsilon}} \bullet \mathbb{B}[\dot{\boldsymbol{\varepsilon}}^g]) \, \mathrm{d}\mathbf{x} \tag{48}$$

an equation that for non-associative flow rule, i.e. $\mathbf{P} \neq \mathbf{Q}$ and $\mathbb{B}$ not possessing the major symmetry, contains *a volume integral*.

Remark 4

Equation (48) highlights a difficulty of the non-associative flow rule, since it implies the presence of a volume integral in the formulation. Since the Green's function (25) and (26) is developed for generality to include the case $\mathbf{P} \neq \mathbf{Q}$, continuing with Equation (48) would provide a formulation for the non-associative flow rule.

In this paper, we restrict the analysis for simplicity to the associative flow rule, $\mathbf{P} = \mathbf{Q}$, so that $\mathbb{B}$ becomes fully symmetric and the domain integral (47) vanishes, yielding the boundary integral equation for velocity:

$$\mathbf{c}^g(\mathbf{y}) \bullet \mathbf{v}(\mathbf{y}) = \int_{\partial \mathscr{B}} [\dot{\boldsymbol{\sigma}}(\mathbf{x})\mathbf{n} \bullet \mathbf{v}^g(\mathbf{x}, \mathbf{y}) - \dot{\boldsymbol{\sigma}}^g(\mathbf{x}, \mathbf{y})\mathbf{n} \bullet \mathbf{v}(\mathbf{x})] \, \mathrm{d}l_x \tag{49}$$

that will be employed in the following. For interior points, the integral equations for velocity gradient and stress can be obtained from Equation (49) in the form

$$v_{g,k}(\mathbf{y}) = \int_{\partial \mathscr{B}} [\mathbf{v} \bullet \dot{\boldsymbol{\sigma}}^g_{,k}(\mathbf{x}, \mathbf{y})\mathbf{n} - \mathbf{v}^g_{,k}(\mathbf{x}, \mathbf{y}) \bullet \dot{\boldsymbol{\sigma}}\mathbf{n}] \, \mathrm{d}l_x \tag{50}$$

and

$$\dot{\sigma}_{ij}(\mathbf{y}) = \int_{\partial\mathscr{B}} (\mathbb{E} - \mathbb{B})_{ijhk}[\mathbf{v} \bullet \dot{\boldsymbol{\sigma}}^h_{,k}(\mathbf{x}, \mathbf{y})\mathbf{n}]\, \mathrm{d}l_x - \int_{\partial\mathscr{B}} \dot{\sigma}^h_{ij}\dot{\sigma}_{hk} n_k\, \mathrm{d}l_x \tag{51}$$

respectively.

Note that for incompressible materials a boundary integral equation is also needed for the in-plane pressure rate. This has been given by Bigoni and Capuani [24] and is not repeated here for conciseness.

4. NUMERICAL STRATEGY

The numerical approach to analyse elastoplastic problems is described below, with reference to the specific material employed in the examples, namely, J_2-flow theory with linear hardening and incompressible elasticity.

- Material:
  - yield function, Equation (27);
  - incremental constitutive equations, Equation (27).
- Infinite-body Green's function set and boundary integral equation for the loading (Equations (37) and (49)) and unloading (Equations (37) and (49) with $\mu = \mu_*$) branches of constitutive equation.
- Domain partition. The domain is divided into a number of subregions of arbitrary shape (rectangular for simplicity in our examples, Figure 1). These subregions are supposed to be characterized at each increment by an infinite-body homogeneous Green's function, in general, different increment by increment. Obviously, each elastic region can be characterized by a single domain and (due to the isotropy assumption) its Green's function is insensitive to orientation of the reference system. On the contrary, volume elements in the plastic zone have been referred in our examples to the principal reference system of stress, since Equation (37) has been employed (see Figure 1); however, it is possible

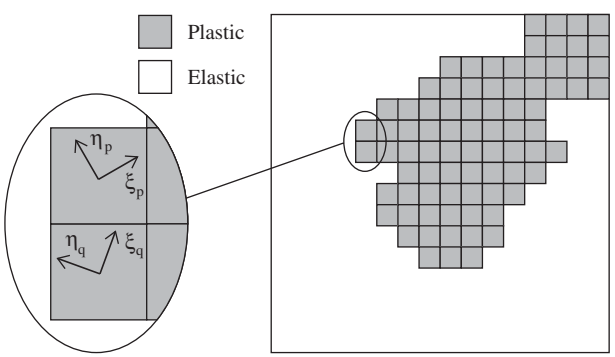

Figure 1. Sketch of the multizone discretization of plastic region.

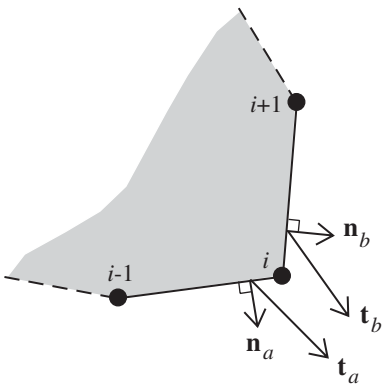

Figure 2. Corner at node i, unit normals $\mathbf{n}_a$, $\mathbf{n}_b$ and tractions $\mathbf{t}_a$ and $\mathbf{t}_b$.

to use a global system common to all elements if the general formulation (16) of the Green's function is employed.

- Incremental solution. The discretized problem at each increment is solved through a multizone boundary element method, detailed later (Section 4.1).
- Integration along a loading path of the incremental solution. Different techniques can be employed here, two of which are detailed later (Section 4.2).

4.1. Multizone technique

The discretized form of Equation (49) is applied separately to every subdomain, taken rectangular for simplicity. Linear shape functions are considered, to represent the boundary fields. All the subregions are combined following a multiregion formulation, based on the observation that continuity of incremental displacements and tractions are to be imposed across adjacent subdomains, namely

$$\mathbf{v}^{i,l} = \mathbf{v}^{j,l} \quad \text{and} \quad \mathbf{t}^{i,l} = -\mathbf{t}^{j,l} \tag{52}$$

at every node l belonging to the neighbouring subdomains i and j.

Related to the fact that tractions are not uniquely defined at a corner, it is well-known that additional unknown tractions arise in the treatment of multidomains and different remedies to this problem have been proposed, for instance, through round-off of the corners [37], or introduction of additional coincident nodes [38, 39], or discontinuous elements [40]. All these methods suffer limitations not acceptable for our purposes, so that we assume the Cauchy stress to be uniquely defined at an internal corner. Therefore, the reciprocity condition

$$\mathbf{t}_a \bullet \mathbf{n}_b = \mathbf{t}_b \bullet \mathbf{n}_a \tag{53}$$

(where $\mathbf{n}_a$ and $\mathbf{n}_b$ are unit normals to different element edges and $\mathbf{t}_a$ and $\mathbf{t}_b$ the relative tractions, Figure 2) is only needed in our two-dimensional setting to solve for the additional unknowns appearing at internal corners, as noted also in Reference [19].

A difficulty with the above-described multidomain method is that sparse final system matrices are generated and sparsity (defined as the number of non-zero elements divided by the total

Table I. Sparsity as a function of the number of subdomains and elements in which subdomain perimeters are discretized.

	No. of elements		
No. of subdomains	8	16	32
1×1	1	1	1
2×2	0.391	0.391	0.383
4×4	0.115	0.113	0.111
8×8	0.0303	0.0299	0.0296
16×16	0.0077	0.0076	0.0076
32×32	0.0019	0.0019	0.0019

number of elements) strongly decreases with the increase of the subdomains number. To explain this point better, let us consider Table I, where the sparsity is reported as a function of the number of subdomains and elements in which the subdomain perimeters have been discretized. In particular, the values of sparsity reported in the table have been generated with our code (that will be detailed later) considering a square domain of unit edge, divided into different subdomains $(1, 4, 16, 64, 256, 1024)$, whose perimeters have been discretized into 8 or 16 or 32 elements. It can be observed from the table that sparsity depends slightly on the discretization of the subdomain perimeters, but strongly on the number of subdomains.

In our examples the matrix is stored as sparse and the final system is solved using the technique proposed by Zlatev *et al*. [29]. In particular, the routine Y12MA, available on http://www.netlib.org/y12m/, has been employed.

4.2. Integration of incremental solutions

Integration along a loading path is required for the solution of elastoplastic problems. We have tested two techniques in our examples, namely, a simple forward Euler scheme and a much more complicated iterative strategy. These are described below. We note however that in all the examples analysed by us the forward Euler scheme performed very well and was found to be largely sufficient to capture the main numerical results.

4.2.1. A forward Euler scheme. The loading path is divided into linear incremental steps of variable size. The size of the steps is selected to meet two requirements:

- allow for a precise transition from elastic to plastic (or vice versa, when needed) of the volume element;
- impose a limit on the maximum possible rotation of the principal stress reference system during plastic deformation.

The latter of the above points is achieved by iteration, adjusting the size of the step until rotation becomes less than a given tolerance, while the former requires a more sophisticated procedure. In particular, at the first step of loading all materials are considered elastic. Therefore, after calculation of the stress field, satisfaction of the yield condition is checked (at the central point of every, say N, subdomains) and the amplitude of the step is re-scaled by the factor α_1

defined as

$$\alpha_1 = \min_{j=1,\ldots,N} \frac{\sqrt{2}\,\sigma_0}{\sqrt{3\,\Delta\mathbf{S}^j \bullet \Delta\mathbf{S}^j}} \tag{54}$$

so that the most stressed subdomain 'touches' yielding. At the generic ith incremental step, the re-scaling factor for the jth elastic subdomain α_i^j is determined as the solution of the equation

$$\frac{\sigma_0^2}{3} = \frac{(\mathbf{S}_{i-1}^j + \alpha_i^j \Delta\mathbf{S}_i^j) \bullet (\mathbf{S}_{i-1}^j + \alpha_i^j \Delta\mathbf{S}_i^j)}{2} \tag{55}$$

where σ_0 is the current value of yielding in uniaxial stress reached by the jth element and $\mathbf{S}_i^j$ is the deviatoric stress at step i relative to the subdomain j. Finally, solving (55) and considering all elastic subdomains N_E yields the re-scaling factor at step i

$$\alpha_i = \min_{j=1,\ldots,N_E} \frac{\sqrt{(\mathbf{S}_{i-1}^j \bullet \Delta\mathbf{S}_i^j)^2 + (\Delta\mathbf{S}_i^j \bullet \Delta\mathbf{S}_i^j)(2\sigma_0^2/3 - \mathbf{S}_{i-1}^j \bullet \mathbf{S}_{i-1}^j)} - \mathbf{S}_{i-1}^j \bullet \Delta\mathbf{S}_i^j}{\Delta\mathbf{S}_i^j \bullet \Delta\mathbf{S}_i^j} \tag{56}$$

4.2.2. An iterative strategy. For any load increment, the solution is determined by iteration to satisfy equilibrium, compatibility and the yield condition at the end of the increment. The adopted process is essentially new, though akin to the iteration schemes usually employed for the finite element method (see e.g. Reference [41]). The procedure is summarized as follows:

(a) Assign a load increment.
(b) Update material parameters and state variables (stress, elastic and plastic deformations and hardening parameters; note that these affect Green's functions and boundary integral equations) with the data available from the previous iteration (the previous load increment at first iteration).
(c) Compute the incremental solution.
(d) All subdomains are now to be evaluated. Let us start considering one of these.
(e) Calculate state variables at certain reference points in the subdomain (see below), where the yield condition is checked. Determination of whether the subdomain is elastic or plastic is needed. In particular:
  - for elastic subdomains. The stress lies:
    - inside the yield surface: set subdomain residual tractions equal to zero and go to (g);
    - outside the yield surface: employ a return mapping algorithm (see below) to compute a new value of state variables and go to (f);
  - for plastic subdomains. The stress lies:
    - on the yield surface: set residual tractions equal to zero and go to (g);
    - outside the yield surface: employ a return mapping algorithm (see below) to compute a new value of state variables and go to (f);
    - inside the yield surface (corresponding to elastic unloading): compute a new value of state variables assuming elastic behaviour and go to (f);

(f) Compute tractions at the boundaries of the subdomain corresponding to the corrected values of state variables (see below). Compute the subdomain residual tractions (i.e. the difference between the tractions calculated at (c) and the correction just evaluated).
(g) If all subdomains have not been considered, take a subdomain not yet analysed and go to (e).
(h) Convergence check: *if* the norm of the residual tractions evaluated on all subdomains is less than a prescribed tolerance: go to (a), *otherwise* apply the residual tractions as a new load increment and go to (b).

There are certain details still to be defined in the above procedure (marked with the note 'see below'), in particular, the reference points were to check satisfaction of the yield criterion, the return mapping, and the way to compute traction corrections at the boundary have to be selected. There is a certain liberty in setting these details and our choices have been dictated by simplicity. In particular, regarding the reference points, the centroid of the subdomain, where the stress and strain are evaluated employing integral equations, has been selected to check the yield condition and update the tangent constitutive operator. Regarding the return mapping algorithm, we have used the cutting-plane algorithm proposed by Simo and Hughes [42]. Finally, the stress evaluated at the centroid of the subdomain is used to update the tractions at the boundary of the subdomain, employing the Cauchy formula $\mathbf{t} = \boldsymbol{\sigma}\mathbf{n}$, where $\mathbf{n}$ is the unit normal to the boundary. This simple procedure has proved to be accurate enough in our examples.

5. NUMERICAL EXAMPLES

Since our boundary element approach is new, numerical examples are important, on the one hand, to validate the formulation and on the other hand to explore capabilities of the method. Therefore, a general-purpose Fortran 90 code for two-dimensional analyses has been developed at the Computational Solid & Structural Mechanics Laboratory of the University of Trento, whose executable is available on http://www.ing.unitn.it/dims/laboratories/comp_solids_structures.php.

The incompressible elastic and plastic J_2-flow theory material with linear (positive) hardening detailed in Section 2.3 has been considered in all the following numerical examples. The material behaviour is very simple; in addition to the elastic shear modulus μ, results are completely characterized by the dimensionless initial yield stress σ_0/μ and hardening coefficient h/μ. The former parameter has been selected to equal $\frac{3}{500}$ in the examples, whereas different values of h/μ have been considered; in particular, $h/\mu = \{0.5, 0.1, 0.01\}$. Since the perfect plasticity limit $h = 0$ coincides with the loss of ellipticity, it is expected that the numerical analyses become less and less accurate at decreasing hardening. This has indeed been observed in the numerical simulations, so that the Gauss points for integration of the singular integrals have been increased as follows: 12 Gauss points for $h/\mu = 0.5$, 48 for $h/\mu = 0.1$, and 60 for $h/\mu = 0.01$.

The choice of the above-described material model has been suggested by the fact long known in the community of finite element developers that the incompressibility constraint poses difficulties in the finite element approach (particularly with reference to fluid dynamics, see e.g. References [43, 44] for a recent review; the specific problem of elastoplasticity, which is of interest here, is addressed in References [31, 32]), which are completely avoided by using

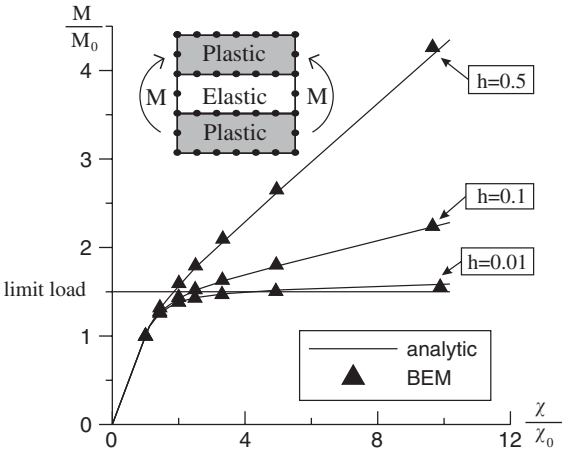

Figure 3. Moment versus curvature for plane-strain bending of a plate (simulations are compared to the analytical solution).

boundary element formulation (see Reference [45] for fluid dynamics and Reference [22] for incompressible elasticity). However, we believe that implementation of different models—under the assumptions of associative flow rule and ellipticity—will be straightforward.

5.1. Bending of a flat, infinite plate

We start with a very simple example for which the analytical solution is known, the plane-strain bending of a square block (of edge $2b$), obtained by imposing rotation of two (initially parallel) edges, maintained plane during bending. In this case, the principal stress directions do not rotate during loading so that iteration is not needed, since the consistency condition is automatically satisfied at the end of every loading step. Note that the boundaries of the elastic zone are *a priori* known to be two segments parallel to an edge of the block. Therefore, a multizone discretization can be avoided and only the contours of the elastic zone and of the two bounding symmetric plastic zones are discretized (in the way sketched in the insert of Figure 3). Edges are meshed with 20 linear elements and loading steps are calibrated to obtain subsequent yielding of one element of the inner elastic core. Results are compared to the analytical solution in Figure 3, where the moment M (divided by the moment at first yielding M_0) is reported as a function of the curvature χ (divided by the curvature at first yielding χ_0). Note that yielding in the figure initiates when $M/M_0 = \chi/\chi_0 = 1$ and that results pertaining to $h/\mu = 0.01$ are very close to the perfectly plastic limit. Beyond the excellent agreement between simulations and numerical solution, the spurious stiffness effects noted for the same problem by Nagtegaal *et al*. [31] are not observed.

5.2. Two punch problems

We analyse the two punch problems investigated also under our same constitutive assumptions by Cervera *et al*. [32], employing finite elements. The two boundary value problems sketched in Figure 4 have been considered: case (a) represents a foundation on a vertical cut, whereas

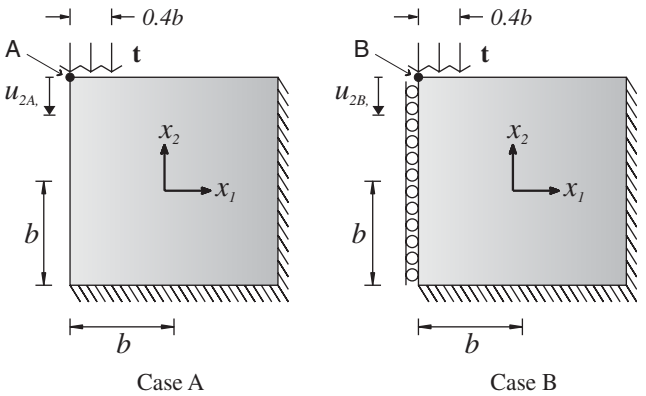

Figure 4. Geometry of the two analysed punch problems: case A is a foundation on a vertical cut and case B is the Prandtl punch problem.

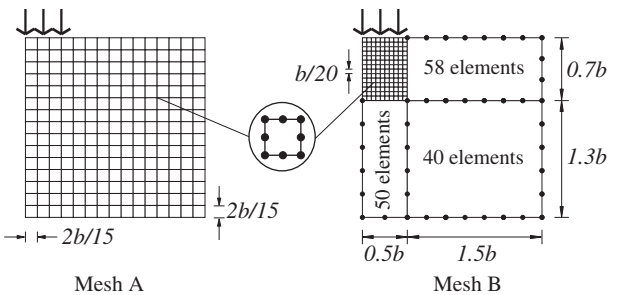

Figure 5. Discretizations employed in the examples. Note the highly inhomogeneous discretization employed in mesh B.

case (b) is the well-known Prandtl punch problem. In the special situation of perfect plasticity, the limit loads for the two problems are[††]

$$(\mathbf{t}_{\lim})_{\mathrm{A}} = \frac{2}{\sqrt{3}}\sigma_0, \quad (\mathbf{t}_{\lim})_{\mathrm{B}} = \frac{2+\pi}{\sqrt{3}}\sigma_0 \tag{57}$$

respectively, which are expected to be numerically approached at decreasing hardening.

To test the capabilities of our method, the geometry A in Figure 4 has been discretized by adopting different meshes, two of which are reported in Figure 5 and the others in detail in Figure 13. The Prandtl problem, case B in Figure 4, has been analysed for conciseness by employing only mesh A (Figure 5). In particular, the uniform mesh A consists of 15×15

[††]A constant stress sector corresponding to null horizontal stress, vertical stress equal to $(\mathbf{t}_{\lim})_{\mathrm{A}}$ and an out-of-planestress equal to $(\mathbf{t}_{\lim})_{\mathrm{A}}/2$ provides Equation $(57)_1$ as a lower bound to the collapse load. The fact that $(\mathbf{t}_{\lim})_{\mathrm{A}}$ provides also an upper bound can be verified by considering a mechanism with a discontinuity plane inclined at 45°. Equation $(57)_2$ can be found in Reference [31].

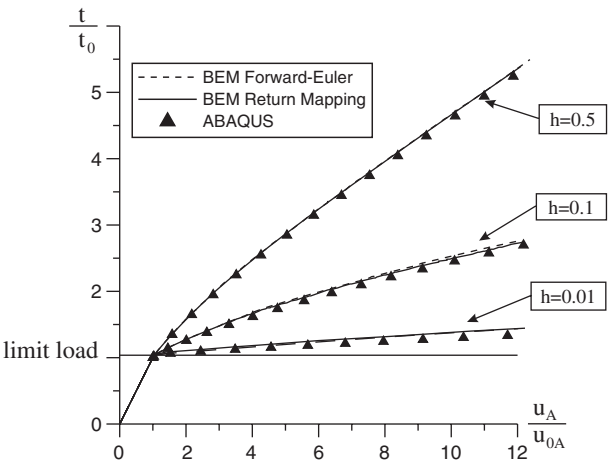

Figure 6. Load (per unit length) versus displacement for a foundation on a vertical cut (our simulations are compared to the ABAQUS solution).

subdomains (themselves discretized into eight linear elements), while the non-uniform mesh B consists of three macro-zones and a region finely subdivided into 14×10 subdomains (themselves discretized into eight linear elements). The macrozones employed in mesh B have to remain elastic during the entire loading program and are discretized along their boundaries through linear elements. Possibility of optimizing discretization employing subdomains widely ranging in size highlights one of the advantages of the boundary element formulation.

The two different integration schemes presented in Section (4.2) have been used. Our results have been compared with simulations obtained employing ABAQUS-Standard (Ver. 6.4-1, Hibbitt, Karlsson and Soresen Inc.), with plane strain, four-nodes bilinear, hybrid elements (CPE4H), adopting the uniform mesh A shown in Figure 5 (finer meshes have been found with ABAQUS to provide almost equivalent results in terms of global force/displacement curves, while performance in terms of internal variables distribution may be slightly improved).

Regarding case A of a foundation on a vertical cut, the load per unit length $\mathbf{t}$ applied to the material and normalized through division by the load at first yielding $\mathbf{t}_0$ is plotted in Figure 6 versus the vertical displacement at point A (Figure 4) divided by displacement at first loading, $u_{\mathrm{A}}/u_{0\mathrm{A}}$. As a consequence of the employed normalization, yielding starts at the point of co-ordinates $\{1, 1\}$ in the graph. Results obtained with the forward Euler (dashed) and the iterative integration schemes are plotted together with ABAQUS simulations (marked by triangles).

The level sets of (the absolute value of the) in-plane pressure divided by the elastic shear modulus p/μ are reported in Figure 7, for low hardening $h/\mu = 0.01$, at different values of the normalized displacement $u_{\mathrm{A}}/u_{0\mathrm{A}} = \{1, 5, 12\}$, so that $u_{\mathrm{A}}/u_{0\mathrm{A}} = 1$ corresponds to first yielding. Moreover, the level sets of the equivalent plastic strain

$$\varepsilon_{\mathrm{equiv}} = \int_{\text{loading path}} \sqrt{\frac{2}{3}\,\dot{\boldsymbol{\varepsilon}}^{\mathrm{p}} \bullet \dot{\boldsymbol{\varepsilon}}^{\mathrm{p}}}\,\mathrm{d}t \tag{58}$$

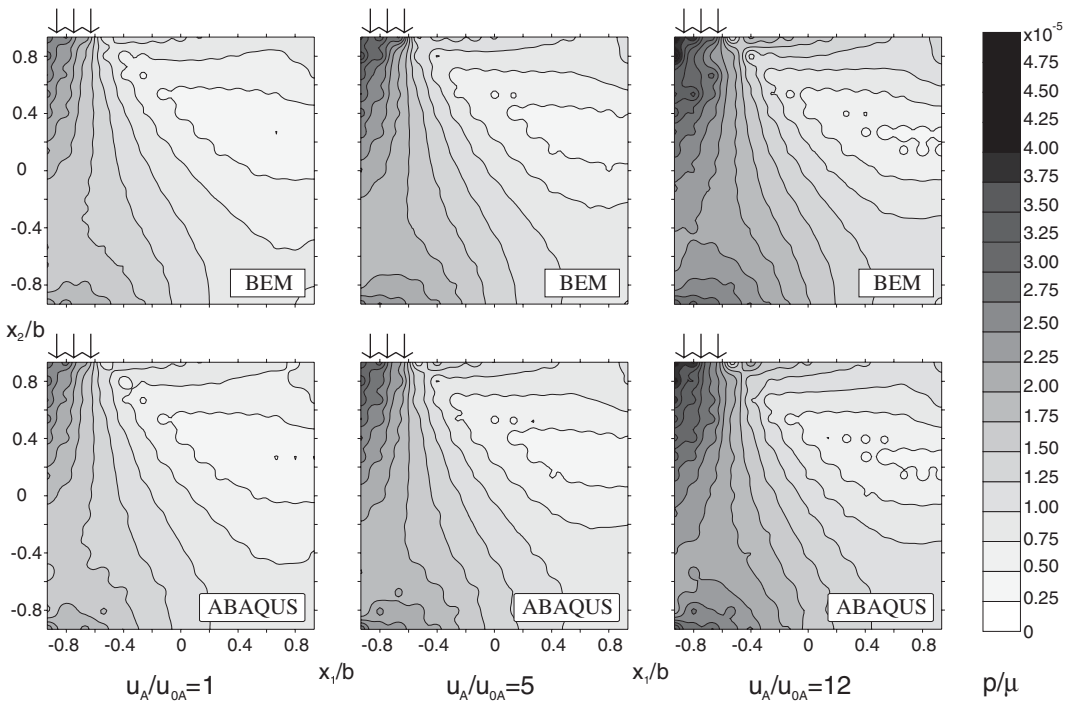

Figure 7. Distribution of pressure for the foundation on the vertical cut at low hardening, $h/\mu = 0.01$ (our simulations are compared to the ABAQUS solution).

have been reported in Figure 8 for $u_A/u_{0A} = \{5, 12\}$ and $h/\mu = 0.01$ (for $u_A/u_{0A} = 1$ the plastic strain is obviously zero). As expected, due to the low hardening assumption, the plastic strain is strongly localized near the foundation, but since load is prescribed instead of displacement at the footing contact, a continuous distribution of strain is found akin to the slip line solution of the perfectly plastic limit. To analyse more closely the plastic zone, this has been detailed as 'mesh A' and 'ABAQUS' in Figure 9 (with reference to the boxes drawn in Figure 8), together with results obtained employing mesh B (Figure 5). It can be noted that the coarse volume discretization gives results close to the ABAQUS solution, whereas the fine discretization provides more accurate results, which have been verified to correspond to an ABAQUS solution employing a fine 40×40 mesh.

The same quantities plotted in the previous Figures 6–8 are now reported in Figures 10–12 for the Prandtl punch problem. In particular, the normalized load versus displacement is reported in Figure 10, whereas level sets of in-plane pressure and effective plastic deformation are plotted in Figures 11 and 12.

We may note from all the above-reported results that the iterative scheme of integration does not much improve the results. Moreover, probably due to the relative simplicity of our constitutive model, we did not note any problem of algorithmic divergence instability, an issue becoming particularly relevant for complicated constitutive setting (see e.g. Reference [46]). However, iteration does affect computing times; with reference to the problem A, we may

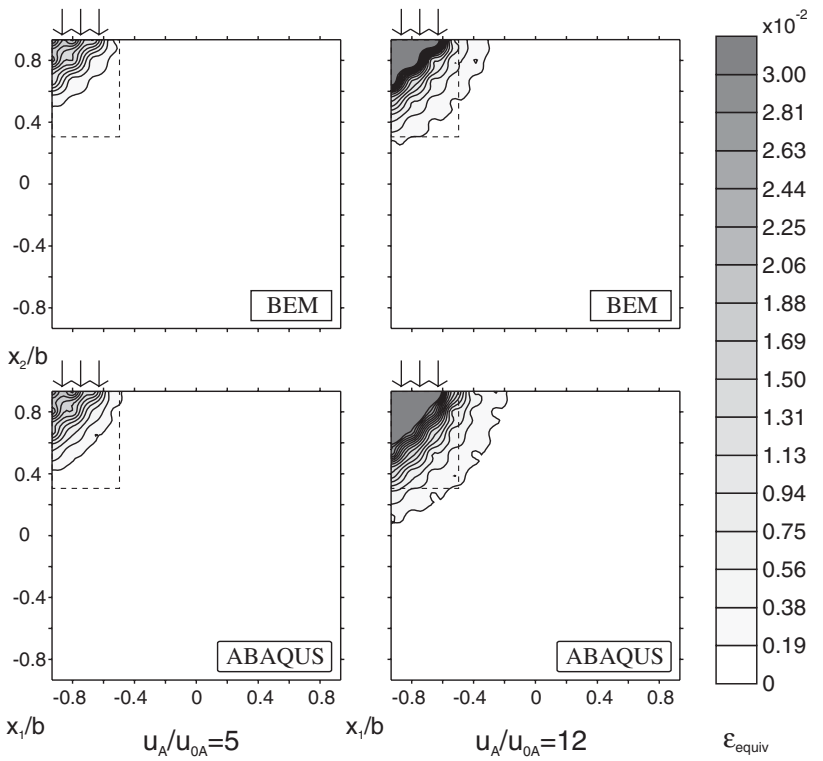

Figure 8. Plastic equivalent strain for a foundation on a vertical cut at low hardening, $h/\mu = 0.01$ (our simulations are compared to the ABAQUS solution). Boxes denote zones detailed in Figure 9.

comment that the iterative scheme consumed 4.3 times the time needed to arrive at $u_A/u_{0A} = 12$ for the uniform mesh A, while speed results improved by a factor 0.8 when results for non-uniform mesh B are compared. Therefore, we may conclude that, at least in the cases considered by us, the explicit integration scheme performed superiorly to the implicit one.

We have also noted that our simulations always provide a slightly stiffer response than that obtained from ABAQUS and the solutions correctly approach the perfect plasticity behaviour at decreasing hardening. Generally speaking, it may be concluded from the figures that the agreement with ABAQUS is excellent, with the maximum differences visible in Figure 12, where the distribution of plastic equivalent strain turns out to be more diffused than in the previous example.

We finally remark that computing times were found to strongly increase with the number of subdomains employed in the volume discretization (for instance, we have observed an increase of a factor up to 50 employing a 40×40 subdomain discretization instead of the 15×15 discretization of mesh A). At the cost of a lower precision in the calculation of the internal fields, we have found that coarse meshes, involving extremely low computing times, can nevertheless be very accurate in evaluating the load/displacement curve. In particular, the two coarse volume discretizations shown in detail in Figure 13 have been employed, one consisting

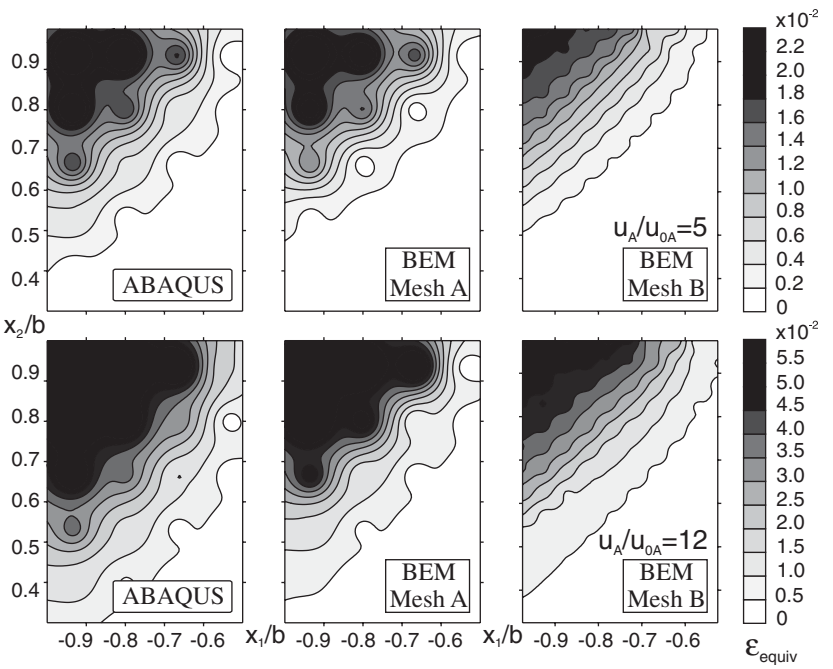

Figure 9. Detail of plastic equivalent strain distribution (see Figure 8) for a foundation on a vertical cut at low hardening, $h/\mu = 0.01$ (our simulations employing meshes A and B, Figure 5, are compared to the ABAQUS solution).

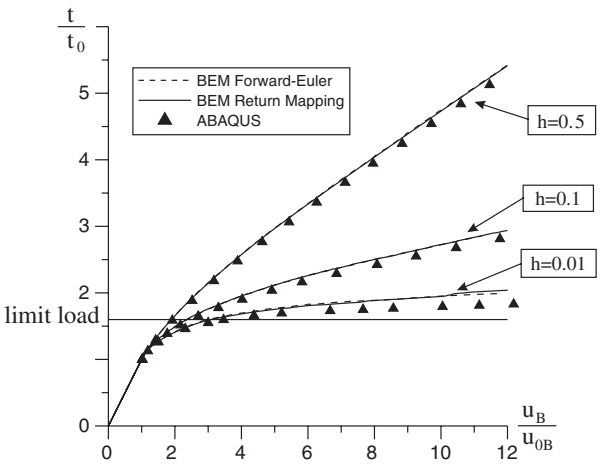

Figure 10. Load (per unit length) versus displacement for the Prandtl punch problem (our simulations are compared to the ABAQUS solution).

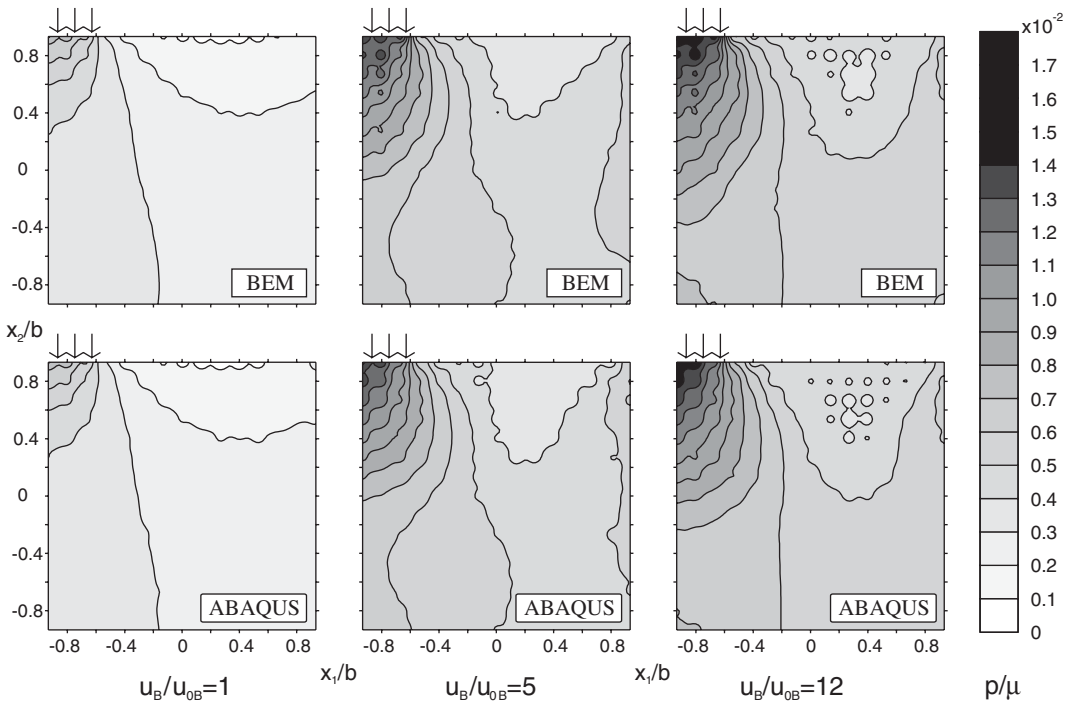

Figure 11. Pressure distribution for the Prandtl punch problem at low hardening, $h/\mu = 0.01$ (our simulations are compared to the ABAQUS solution).

of 5×5 square subdomains (mesh C) and the other of 2×2 macroelements of different sizes (mesh D). It is clear from Figure 13, where the computed load versus displacement curves are reported for meshes A, C, and D, that the results are almost coincident, but the computing times (compared to that relative to mesh A) fall to $\frac{1}{24.7}$ for mesh C and $\frac{1}{54.8}$ for mesh D. It may also be added that for the two coarse meshes the results are obtained with only two incremental steps.

5.3. Two rectangular holes in an infinite elastic–plastic material

To highlight the characteristics of the proposed method, we present the analysis of an infinite elastic–plastic medium containing two rectangular holes and loaded under plane strain condition, by imposing constant displacements on certain portions of the hole contours. The geometry of the problem, together with the volume and surface discretizations are shown in Figure 14. Note that the central rigid plate is displaced to the right the same amount that the two rigid plates are displaced to the left. Since the plastic zone is expected to be highly localized, the volume discretization is very small, so that 8×32 zones have been used. Therefore, this example clearly shows one of the advantages of the boundary element technique. In addition, the consideration of the infinite domain and corners results to be straightforward. In particular, 136 elements

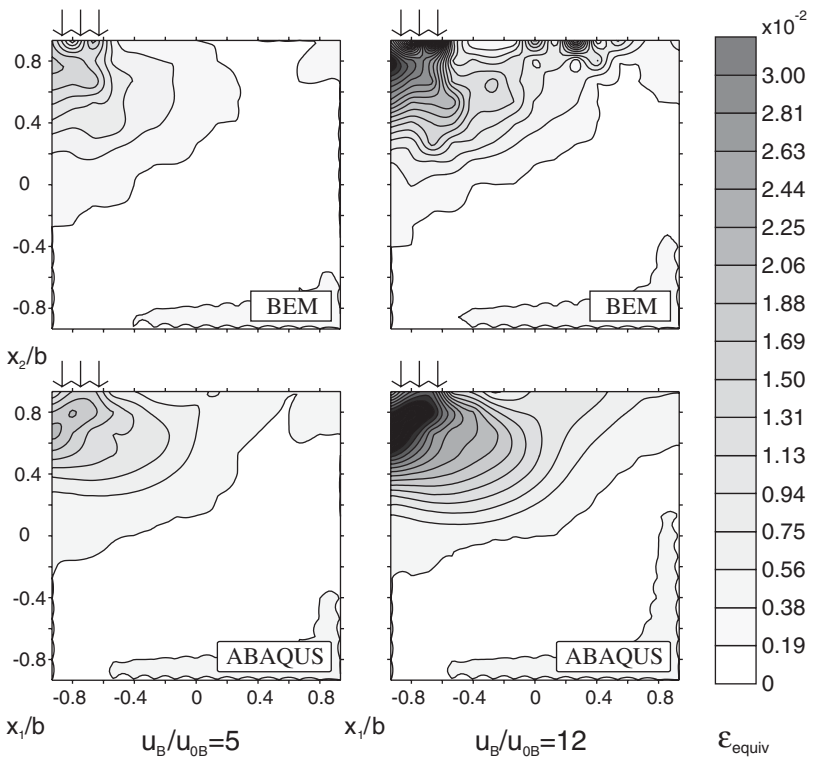

Figure 12. Plastic equivalent strain for the Prandtl punch problem at low hardening, $h/\mu = 0.01$ (our simulations are compared to the ABAQUS solution).

have been employed to discretize the external contour of the holes and two macro-subdomains of 48 elements each have been employed to connect the contour to the volume discretization.

Results pertaining to low hardening $h/\mu = 0.01$ and $\sigma_0/\mu = 3/500$ have been plotted in Figures 15 and 16 in terms of von Mises stress and equivalent plastic strain, respectively. The von Mises stress is reported in the left part of Figure 15 at first yielding and corresponding to $u/u_0 = 1$, where u is the horizontal displacement of the rigid central plate. The central and right parts of the figure pertain to two different levels of load, corresponding to $u/u_0 = 4$ and 6, respectively. Since at first yielding the equivalent plastic strain is obviously null, the left part of Figure 16 refers to $u/u_0 = 2$, while the central and right parts correspond to the same values of u/u_0 employed in Figure 15.

It can be noted from Figure 15 that the stress is concentrated in the internal 'ligament', so that the infinite zone remains almost unstressed. In particular, the stress distribution evidences a sort of 'arc effect' joining the three rigid loading platens. The plastic deformation results from Figure 16 to be localized along well-defined zones, resembling the shear bands formally possible only at the perfectly plastic limit.

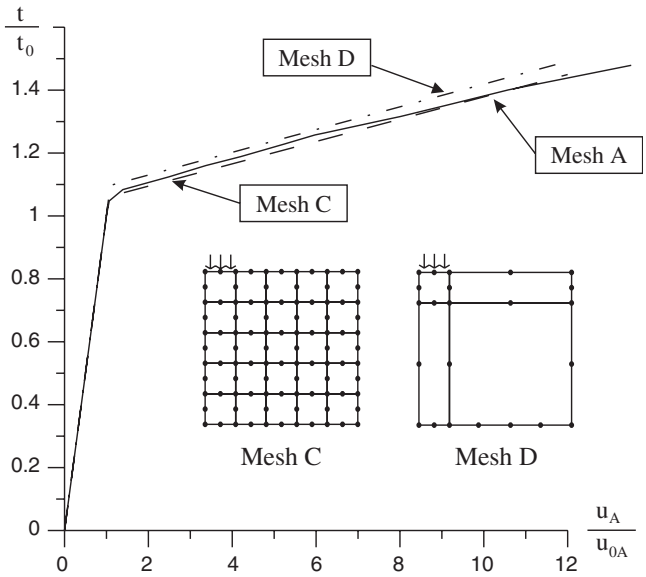

Figure 13. Load (per unit length) versus displacement for a foundation on a vertical cut. The two meshes shown in the figure have been used together with mesh A (5).

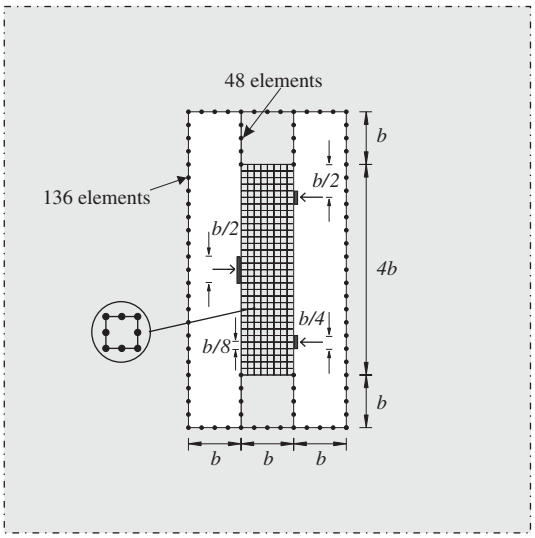

Figure 14. Geometry and discretizations used to analyse a problem of two rectangular holes in an infinite elastic–plastic material loaded in the internal ligament.

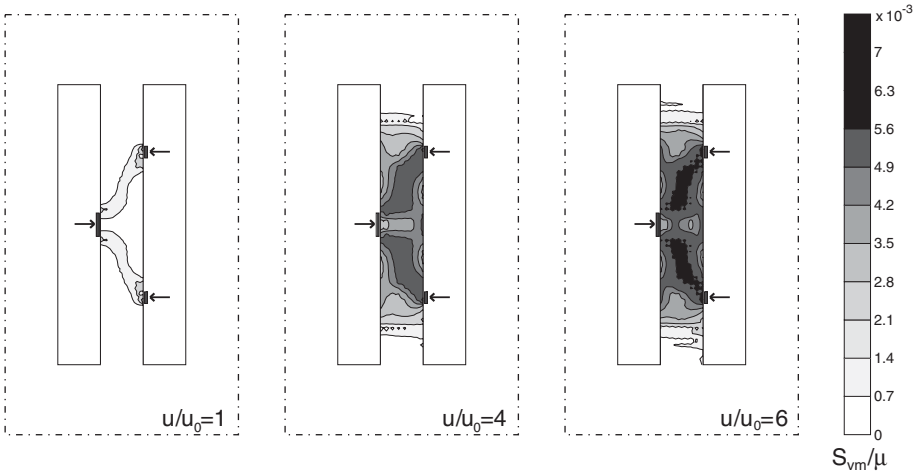

Figure 15. Von Mises stress distribution for the problem sketched in Figure 14 for three different load levels.

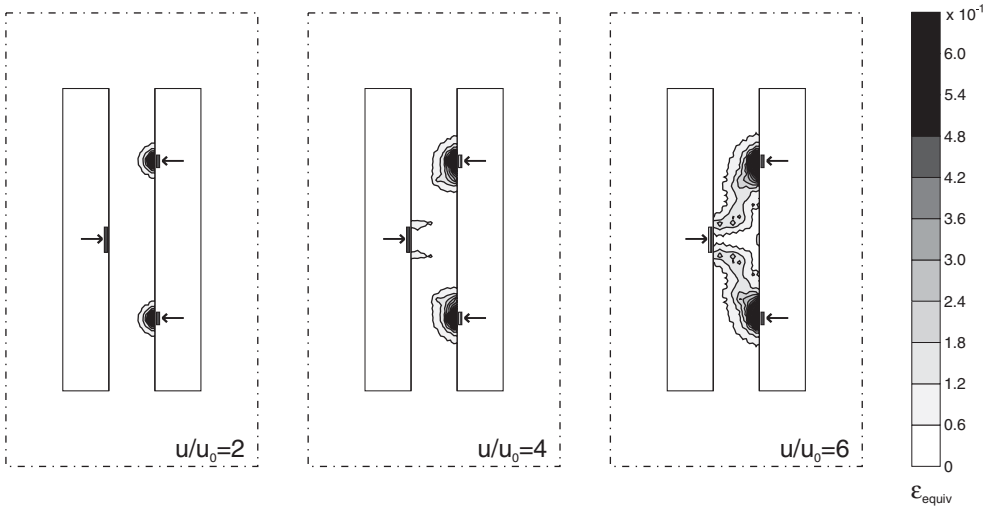

Figure 16. Equivalent plastic strain distribution relative to the problem sketched in Figure 14 for three different load levels.

6. CONCLUSIONS

A novel boundary element technique has been presented in which the plastic and elastic branches of the tangent constitutive operator are treated separately by employing appropriate Green's functions and boundary integral equations. This technique retains all the advantages

connected with the boundary element formulation (volume discretization of the plastic zone only, possibility of analysing incompressibility and singularities) but presents also a series of advantages when compared with the other approaches currently in use, in particular:

> first, domain integrals are avoided; second, since the loading branch of the constitutive operator is formally analogous to a special type of elastic anisotropic constitutive tensor, the method is developed as a straightforward application of multidomain techniques for linear constitutive operators, so that 'special expedients' are not needed.

Several examples demonstrate that the method is powerful and precise enough to provide results perfectly comparable with those provided by commercial codes. Nevertheless, much work remains to be done to bring the proposed method to the same level of generality of other approaches. In particular, different important generalizations would be important, including (in order of increasing complexity):

- inclusion of a large strain formulation;
- treatment of non-associative elastoplasticity;
- analysis of perfect plasticity and softening.

We have shown that difficulties connected to treatment of a non-associative flow rule are related to the boundary integral equations which in this case necessarily include a volume term, while determination of the Green's function does not pose problems (and indeed we have provided a general formula covering non-associativity). Note also that the inclusion of softening would possibly require departure from ellipticity, a situation difficult to be envisaged. In addition to the above, there are other points that would merit a systematic exploration.[‡‡] We believe that implementation and testing of the following features (in order of increasing complexity) should be not particularly difficult but useful to extend the validity of the method:

- parallelization of the code;
- optimization of numerical integration of the Green's functions;
- test of different iterative algorithms to enforce the yield condition;
- test of capabilities of analysing shear bands still within the elliptic domain (in the way pointed out in References [23, 24]);
- inclusion of various constitutive models, still within the hypotheses of ellipticity and flow rule associativity;
- definition of an automatic remeshing strategy of elastic and plastic zones (this will optimize both precision and computing time);
- development of a three-dimensional formulation.

It may be concluded that the performance of the proposed numerical method is sufficiently encouraging to stimulate further developments.

[‡‡]Another aspect that would be worth investigating is the possibility of giving a symmetric Galerkin formulation (see e.g. Reference [47]) for the proposed methodology. This is complicated by the fact that a boundary integral representation for the tractions is currently not available for the constitutive equations employed in the present article. Some steps in this direction have been made by Capuani *et al.* [48], in the simple case of Stokes flow.

APPENDIX A: GREEN'S FUNCTION FOR ISOTROPIC LINEAR ELASTIC MATERIAL

An isotropic linear elastic material is defined by

$$\mathbb{C} = \lambda \mathbf{I} \otimes \mathbf{I} + 2\mu \mathbb{S} \tag{A1}$$

where λ and μ are the Lamé constants and $\mathbb{S}$ is the symmetrizing fourth-order tensor, so that the acoustic tensor $\mathbf{A}(\mathbf{n})$ and its inverse $\mathbf{A}(\mathbf{n})^{-1}$ take the form

$$\mathbf{A}(\mathbf{n}) = (\lambda + \mu)\mathbf{n} \otimes \mathbf{n} + \mu \mathbf{I}, \quad \mathbf{A}^{-1}(\mathbf{n}) = -\frac{\lambda + \mu}{\mu(\lambda + 2\mu)} \mathbf{n} \otimes \mathbf{n} + \frac{1}{\mu} \mathbf{I} \tag{A2}$$

Equation (8) provides the Green's function in the form

$$u_t^g(\hat{r}, \theta) = -\frac{1}{4\pi^2 \mu} \oint_0^{2\pi} \left[\delta_{tg} + \frac{\lambda + \mu}{\lambda + 2\mu} \cos\left(\alpha + \theta + (1 - g)\frac{\pi}{2}\right) \cos\left(\alpha + \theta + (1 - t)\frac{\pi}{2}\right) \right] (\log \hat{r} + \log |\cos \alpha|) \, \mathrm{d}\alpha \tag{A3}$$

which, using the relations

$$\int_0^{\pi/2} \log(\cos \alpha) \left\{ \begin{matrix} \cos^2 \alpha \\ \sin^2 \alpha \end{matrix} \right\} \mathrm{d}\alpha = \frac{\pi}{8}(\pm 1 - \log 4) \tag{A4}$$

and neglecting constant terms, yields finally

$$u_t^g = -\frac{1}{8\pi\mu(1 - \nu)} \left[\delta_{tg}(3 - 4\nu) \log \hat{r} - \cos\left(\theta + (1 - g)\frac{\pi}{2}\right) \cos\left(\theta + (1 - t)\frac{\pi}{2}\right) \right] \tag{A5}$$

where ν denotes the Poisson's ratio.

ACKNOWLEDGEMENTS

Financial support of MURST-Cofin 2004 (Microstructural problems and models: applications in structural and civil engineering) is gratefully acknowledged.

REFERENCES

1. Swedlow JL, Cruse TA. Formulation of boundary integral equations for three dimensional elastoplastic flow. *International Journal of Solids and Structures* 1971; **7**:1673–1683.
2. Mukherjee S. Corrected boundary integral equations in planar thermoplasticity. *International Journal of Solids and Structures* 1977; **13**:331–335.
3. Maier G. On elastoplastic analysis by boundary elements. *Mechanics Research Communications* 1983; **10**: 45–52.
4. Telles JCF. *The Boundary Element Method Applied to Inelastic Problems*. Springer: Berlin, 1983.
5. Bonnet M, Mukherjee S. Implicit BEM formulation for usual and sensitivity problems in elasto-plasticity using the consistent tangent operator concept. *International Journal of Solids and Structures* 1996; **33**: 4461–4480.
6. Frangi A, Maier G. Dynamic elastic–plastic analysis by a symmetric Galerkin boundary element method with time-independent kernels. *Computer Methods in Applied Mechanics and Engineering* 1999; **171**:281–308.
7. Hatzigeorgiou GD, Beskos DE. Dynamic elastoplastic analysis of 3-D structures by the domain/boundary element method. *Computers and Structures* 2002; **80**:339–347.

8. Benallal A, Fudoli CA, Venturini WS. An implicit BEM formulation for gradient plasticity and localization phenomena. *International Journal for Numerical Methods in Engineering* 2002; **53**:1853–1869.
9. Maier G, Miccoli S, Novati G, Perego U. Symmetric Galerkin boundary-element method in plasticity and gradient plasticity. *Computers and Structures* 1995; **17**:115–129.
10. Sladek J, Sladek V, Bazant ZP. Non-local boundary integral formulation for softening damage. *International Journal for Numerical Methods in Engineering* 2003; **57**:103–116.
11. Bui HD. Some remarks about the formulation of three-dimensional thermoelastoplastic problems by integral equations. *International Journal of Solids and Structures* 1978; **14**:935–939.
12. Chandra A, Mukherjee S. An analysis of large strain viscoplasticity problems including the effects of induced material anisotropy. *Journal of Applied Mechanics* 1986; **53**:77–78.
13. Chen ZQ, Ji X. A new approach to finite deformation problems of elastoplasticity boundary element analysis method. *Computer Methods in Applied Mechanics and Engineering* 1990; **78**:1–18.
14. Jin H, Runesson K, Mattiasson K. Boundary element formulation in finite deformation plasticity using implicit integration. *Computers and Structures* 1989; **31**:25–34.
15. Okada H, Rajiyah H, Atluri SN. Some recent developments in finite-strain elastoplasticity using the field-boundary element method. *Computers and Structures* 1988; **30**:275–288.
16. Okada H, Rajiyah H, Atluri SN. A full tangent stiffness field-boundary element formulation for geometric and material non-linear problems of solid mechanics. *International Journal for Numerical Methods in Engineering* 1990; **29**:15–35.
17. Aliabadi MH. *The Boundary Element Method*, *vol. 2*, *Applications in Solids and Structures*. Wiley: Chichester, 2002.
18. Sladek V, Sladek J. Displacement gradients in BEM formulation for small strain plasticity. *Engineering Analysis with Boundary Elements* 1999; **23**:471–477.
19. Gao X-W, Davies TG. An effective boundary element algorithm for 2D and 3D elastoplastic problems. *International Journal of Solids and Structures* 2000; **37**:4987–5008.
20. Maier G, Miccoli S, Novati G, Sirtori S. A Galerkin symmetric boundary-element method in plasticity: formulation and implementation. In *Advances in Boundary Element Techniques*, Kane JH, Maier G, Tosaka N, Atluri SN (eds). Springer: New York, 1992; 288–328.
21. Henry DP, Banerjee PK. A new BEM formulation for two- and three-dimensional elastoplasticity using particular integrals. *International Journal for Numerical Methods in Engineering* 1988; **26**:2079–2096.
22. Brun M, Capuani D, Bigoni D. A boundary element technique for incremental, non-linear elasticity. Part I: formulation. *Computer Methods in Applied Mechanics and Engineering* 2003; **192**:2461–2479.
23. Brun M, Bigoni D, Capuani D. A boundary element technique for incremental, non-linear elasticity. Part II: bifurcation and shear bands. *Computer Methods in Applied Mechanics and Engineering* 2003; **192**:2481–2499.
24. Bigoni D, Capuani D. Green's function for incremental non-linear elasticity: shear bands and boundary integral formulation. *Journal of the Mechanics and Physics of Solids* 2002; **50**:471–500.
25. Willis JR. Self-similar problems in elastodynamics. *Philosophical Transactions of the Royal Society of London*, *Series A* 1973; **274**:435–491.
26. Willis JR. Inclusions and cracks in constrained anisotropic media. In *Modern Theory of Anisotropic Elasticity and Applications*, Wu JJ, Ting TCT, Barnett DM (eds). SIAM: Philadelphia, PA, 1991; 87–102.
27. Bigoni D, Capuani D. Time-harmonic Green's function and boundary integral formulation for incremental non-linear elasticity: dynamics of wave patterns and shear bands. *Journal of the Mechanics and Physics of Solids* 2005; **53**:1163–1187.
28. Piccolroaz A, Bigoni D, Willis JR. A dynamical interpretation of flutter instability in a continuous medium. 2005, submitted.
29. Zlatev Z, Wasniewski J, Schaumburg K. *Y12M—Solution of Large and Sparse Systems of Linear Algebraic Equations*. Springer: Berlin, Heidelberg, New York, 1981.
30. Bigoni D, Capuani D, Bonetti P. A boundary element technique for incremental, non-linear time-harmonic dynamic elasticity. Part I: formulation, submitted.
31. Nagtegaal JC, Parks DM, Rice JR. On numerically accurate finite element solutions in the fully plastic range. *Computer Methods in Applied Mechanics and Engineering* 1974; **4**:153–177.
32. Cervera M, Chiumenti M, Valverde Q, Agelet de Saraciba C. Mixed linear/linear simplicial elements for incompressible elasticity and plasticity. *Computer Methods in Applied Mechanics and Engineering* 2003; **192**:5249–5263.
33. Gelfand IM, Shilov GE. *Generalized Functions*, *Properties and Operations*, vol. 1. Academic Press: New York, 1964.

34. Needleman A. Non-normality and bifurcation in plane strain tension or compression. *Journal of the Mechanics and Physics of Solids* 1979; **27**:231–254.
35. Bigoni D. Bifurcation and instability of non-associative elastic–plastic solids. In *Material Instabilities in Elastic and Plastic Solids*, Petryk H (ed.). CISM Lecture Notes No. 414. Springer: Wien, New York, 2000; 1–52.
36. Benallal A, Bigoni D. Effects of temperature and thermo-mechanical couplings on material instabilities and strain localization of inelastic materials. *Journal of the Mechanics and Physics of Solids* 2004; **52**:725–753.
37. Jaswon MA, Symm GT. *Integral Equation Methods in Potential Theory and Elastostatic*. Academic Press: London, 1977.
38. Chaudonneret M. On the discontinuity of the stress vector in the boundary integral equation method for elastic analysis. In *Recent Advances in Boundary Element Methods*, Brebbia CA (ed.). Pentech Press: London, 1978; 185–194.
39. Zhang Q, Mukherjee S. Design sensitivity coefficients for linear elastic bodies with zones and corners by the derivative boundary element method. *International Journal of Solids and Structures* 1991; **27**:983–998.
40. Wilde AJ. A hypersingular dual boundary element formulation for three-dimensional fracture analysis. *Ph.D. Thesis*, Wessex Institute of Technology, University of Wales, U.K., 1998.
41. Besseling JF, van der Giessen E. *Mathematical Modelling of Inelastic Deformation*. Chapman & Hall: London, 1994.
42. Simo JC, Hughes TJR. General return mapping algorithms for rate-independent plasticity. In *Constitutive Laws for Engineering Materials*, Desai CS (ed.). Elsevier: New York, 1987.
43. Zienkiewicz OC, Taylor RL. *The Finite Element Method* (4th edn). McGraw-Hill: New York, 1989.
44. Dvorkin EN. On the convergence of incompressible finite element formulations. *Engineering Computations* 2001; **18**:539–556.
45. Pozrikidis C. *Introduction to Theoretical and Computational Fluid Dynamics*. Oxford University Press: New York, 1997.
46. Sloan SW, Abbo AJ, Sheng D. Refined explicit integration of elastoplastic models with automatic error control. *Engineering Computations* 2001; **18**:121–154.
47. Bonnet M, Maier G, Polizzotto C. Symmetric Galerkin boundary element methods. *Applied Mechanics Review* 1998; **51**:669–704.
48. Capuani D, Bigoni D, Brun M. Integral representations at the boundary for Stokes flow and related symmetric Galerkin approximation. *Archives of Mechanics*, 2005, in press.
49. Bonnet M. *Boundary Integral Equation Methods for Solids and Fluids*. Wiley: New York, 1995.
50. Venturini WS. *Boundary Element Method in Geomechanics*. Springer: Berlin, 1983.

